379
N81d
No. 1704

LOW-VELOCITY K-SHELL IONIZATION CROSS SECTIONS FOR PROTONS, DEUTERONS, AND ALPHA PARTICLES BOMBARDING THIN METAL TARGETS

DISSERTATION

Presented to the Graduate Council of the
North Texas State University in Partial
Fulfillment of the Requirements

For the Degree of

DOCTOR OF PHILOSOPHY

By

Roger Karl Rice, M. S.
Denton, Texas

May, 1981

Y544

Rice, Roger K., Low Velocity K-Shell Ionization Cross Sections for Protons, Deuterons, and Alpha Particles Bombarding Thin Metal Targets. Doctor of Philosophy (Physics), May, 1981, 61 pp., 5 tables, bibliography, 48 titles.

The purpose of this work was to examine the effect of the use the assumption $\hbar\omega_{2K}/E_{CM} << 1$ in calculating K-shell ionization cross sections in the plane wave Born approximation (PWBA) where $\hbar\omega_{2K}$ is the observed binding energy of the K-shell and E_{CM} is the energy of the incident particle in the center of mass system. Avoiding this assumption produces a threshold for ionization at $E_{CM} = \hbar\omega_{2K}$. Calculations employing the assumption, which leads to the use of approximate limits of integration, do not go to zero for even the lowest values of the incident energy.

This threshold effect was examined theoretically by calculating cross sections in the PWBA and perturbed stationary state (PSS) theories with both the exact and approximate limits of integration near the experimental limit which corresponds to $\hbar\omega_{2K}/E_{CM} \leq 0.1$. Two Coulomb deflection factors (C_K and C_B) and two relativistic corrections (R_A and R_B) were also studied.

Cross sections for K-shell x-ray production were measured for protons, deuterons, and alpha particles incident on thin solid foils of $_{29}Cu$, $_{41}Nb$, $_{47}Ag$, and $_{51}Sb$ in the same energy region for comparison with theoretical predictions.

Cross sections calculated with the exact limits PWBA(Ex) were lower than those calculated with approximate limits by

$\sim$25% at the lowest velocities for protons. Measured absolute values for the cross sections differed from the theoretical values by much more than this. In general the measured values were within experimental uncertainties of two theoretical calculations ($C_B PSSR_A$ and $C\ PSSR_B$) at the highest energies. Due to the large difference in energy dependence between measured and theoretical values at low energy, however, the measured values fell below the predictions of the $C_B PSSR_{A,B}$ and approached the $C_K PSSR_{A,B}$.

A measure of the Coulomb deflection factor derived by dividing the measured cross section values by the predictions of the PSSR shows similar disagreement with both theoretical calculations. Ratios of measured cross sections for deuteron and proton bombardment, which isolates the Coulomb deflection effect, shows the same disagreement with both theoretical calculations. Ratios calculated with exact and approximate limits differ by less than experimental uncertainties. Ratios of measured cross sections for ^4_2He and ^2_1D bombardment, which isolate the binding effect, show good agreement with the theoretical predictions. Ratios of relative experimental and theoretical cross section values normalized to unity at high velocity show how well the calculations predict the velocity dependence of the data. The two theoretical calculations which show the best agreement with result of experiment fail to predict the velocity dependence of the data.

In conclusion, the threshold effect seems to be too small to be measured in this energy region. The two relativistic calculations studied are almost identical and seem to provide adequate results. The increased binding effect calculation provides good agreement with the data. The two Coulomb deflection effect calculations differ in both energy dependence and magnitude from the measured data at low velocities.

TABLE OF CONTENTS

LIST OF TABLES

LIST OF ILLUSTRATIONS

CHAPTER I

INTRODUCTION

Inner-shell ionization produced by ion impact has been studied both experimentally and theoretically in recent years.[1-35] The two primary mechanisms for producing inner-shell vacancies are Coulomb ionization[1,3] and electron promotion.[5,12] For Coulomb ionization the vacancy is produced due to the interaction between the nucleus of the incident ion and the target electron. Electron promotion refers to the transition between the quasimolecular states which are formed during slow collisions. These two excitation mechanisms are believed to be important only for certain ranges of the parameters Z_1/Z_2 and v_1/v_e where Z_1 and Z_2 are the atomic numbers of the incident ion and target atom, respectively, and v_1 and v_e are the ion velocity and target electron velocity, respectively. Coulomb ionization is dominant for $Z_1/Z_2 \ll 1$ or $v_1/v_e \gtrsim 1$ and electron promotion is important when $Z_1/Z_2 \sim 1$ and $v_1/v_e \ll 1$. For heavier incident ions, where $Z_1/Z_2 \sim 1$ and $v_1/v_e \lesssim 1$, K-shell electron transfer to bound states of the projectile has been found to be very important in target K-vacancy production.[24,26] In the Z_1/Z_2 and v_1/v_e regions of this work, direct Coulomb ionization, as opposed to electron transfer or excitation,[22] is the dominant mechanism and, therefore, electron promotion, electron excitation and electron transfer to the projectile will not be discussed.

Three theoretical approaches have been widely used to describe direct Coulomb ionization, the binary encounter approximation (BEA),[8,18] the semiclassical approximation (SCA)[4,17] and the plane wave Born approximation (PWBA).[1,3,5,27] All give reasonable estimates for the K-shell ionization cross sections for ions with $Z_1 \leq 4$ incident on high Z_2 ($Z_2 \gtrsim 30$) target atoms at energies of a few MeV.[15,16]

For high Z_1 ($Z_1 > 4$) ions or low Z_2 ($Z_2 \lesssim 30$) targets at lower velocities, however, these calculations overpredict the measurements.[21,28,29] This has been attributed to Coulomb deflection of the incident ion by the target nucleus and also to increased binding of the target electron due to the presence of the projectile inside the K-shell. The BEA and the PWBA have been modified to take Coulomb deflection and increased binding[7,13,14] into account. Further, the PWBA has been modified to include polarization of the target electron wave function by the projectile by appeal to perturbed stationary state (PSS) theory.[10,11,32] The PSS theory also reproduces the original modification for increased binding energy.

All of the calculations discussed so far use non-relativistic single electron wave functions. For heavy targets and low incident ion velocities electronic relativistic effects become important. Several relativistic correction factors have been calculated as functions of velocity and Z_2 and have been applied to the above theories.[2,9,13,30,31]

The PWBA modified for Coulomb deflection, increased binding,

polarization, and relativistic effects has provided good predictions of measured x-ray production cross sections for $Z_1/Z_2<<1$.[19-31,23,25,28,29]

It has been shown that the PWBA and the PSS theories exhibit a universal behavior[14,32] when plotted as functions of the reduced velocity and binding energy parameters η and θ, respectively. Most of the experimental data available corresponds to $(\eta/\theta^2)>.02$. Recent works[29,33,34] at low velocities for which $\eta/\theta^2<.02$ show discrepancies between theory and experiment in the energy dependence of ionization by protons and alpha particles incident on high Z_2 targets.

For protons incident on high Z_2 targets with $\eta/\theta^2<.02$, one of the simplifying assumptions used to evaluate cross sections in the PWBA is no longer valid. This assumption is $\hbar\omega_{2k}/E_{CM}<<1$, where $\hbar\omega_{2k}$ is the K-shell binding energy of the target atom and E_{CM} is the energy of the incident projectile in the center of mass system. It has been suggested[34] that the invalidity of this assumption is the reason for the discrepancies in the theoretical and experimental cross sections observed in this energy region. Basbas[22] points out that this assumption is the reason for the dependence of the cross section on the projectile velocity v_1, and not on the energy E_1 (no mass dependence). This assumption is also responsible for the absence of a "threshold effect" in the energy dependence of the ionization cross sections calculated using the approximate limits. This means that cross sections calculated in the PWBA while assuming $\hbar\omega_{2k}/E_{CM}<<1$ do not

go to zero for values of E_1, which are less than the binding energy of the target electron.

The purpose of this work is to examine this threshold effect both theoretically and experimentally. To test the importance of this approximation, calculations were made in the PWBA without assuming $\hbar\omega_{2k}/E_{CM}<<1$. The magnitude of the effect of this approximation was studied in the projectile energy region corresponding to $\hbar\omega_{2k}/E_{CM} \leq 0.1$. To do so, K-shell x-ray production cross sections for protons (^1_1H), deuterons (^2_1D) and alpha particles (^4_2He) incident on thin solid targets of $_{29}Cu$, $_{41}Nb$, $_{47}Ag$ and $_{51}Sb$ in the same projectile energy region have been measured.

The reasons for using these three projectiles are as follows:

(1) Protons and deuterons have the same Z_1 and, therefore, at the same velocity, they have the same increased binding effect;

(2) Deuterons and alpha particles have the same charge to mass ratio and, therefore, at the same velocity they have the same Coulomb deflection effect;

(3) These ratios allow the cancellation of certain experimentally measured quantities which make ratio values more accurate quantities than absolute cross section measurements.

By taking ratios of cross sections for proton bombardment to cross sections for deuteron bombardment the Coulomb deflection effect can be isolated and compared to theoretical calculations. Similarly, the ratio of alpha particle induced cross sections to deuteron induced cross sections give a measure of the increased binding effect.

Typical thin-target cross sections have absolute uncertainties of about 10 - 15%, yet many published values from different experimenters vary by much more than this range.[35] For this reason it is sometimes difficult to assess theoretical calculations which differ by less than the discrepancies between experimental values. In this regard it is sometimes more revealing to test the energy dependence of theoretical models by normalizing theory and experiment to unity at a given value of the incident energy and comparing relative experimental values which do not include large normalization uncertainties. In this work both absolute and relative experimental values are used to test the different theoretical calculations.

Only PWBA and PSS calculations will be discussed in detail and compared to experimental values because the SCA and the PWBA are identical for $\hbar\omega_{2K}/E_{CM} \ll 1$, and no BEA calculations in this energy region have been published.

CHAPTER II

THEORY

As mentioned earlier only the PWBA and PSS theories will be discussed in detail. Though the PSS is cast in terms of the PWBA with scaled variables, it is the result of using perturbed stationary states to describe the target atoms to account for increased binding and polarization effects. The first part of this chapter describes the origin of the PWBA. This is followed by a description of the evaluation of the PWBA with the relaxation of the approximation $\hbar\omega_{2k}/E_{CM}<<1$. A brief description of the increased binding and polarization effect, two coulomb deflection calculations, and two relativistic effects calculations are also included.

PWBA

The PWBA is a quantum mechanical description of inner-shell ionization by fast ions derived in 1930 by Bethe.[1] In the transition matrix element the exact eigenfunction is replaced by the product of a plane wave and an unperturbed atomic state. The PWBA is considered to be valid for the ionization process if the incident ion is in the high velocity range, where $(Z_1e^2/\hbar v_1)<<1$, so that the initial and final particle states can be treated as plane waves, and the atomic number of the incident ion Z_1 is much less than the atomic number of the target Z_2 so that the interaction is weak.

With these conditions satisfied, the cross section is proportional to the square of the transition matrix given by[1]

$$V_{fi} = \langle \Phi_{Kf}(\vec{r}_1)\Psi_f(\vec{r}_2) \mid \frac{1}{\vec{r}_1-\vec{r}_2} \mid \Phi_{Ki}(\vec{r}_1)\Psi_i(\vec{r}_2)\rangle \qquad \text{(II.1)}$$

where $\Psi_i(\vec{r}_2)$ is the initial atomic state of the target electron, $\Psi_f(\vec{r}_2)$ is the final state of the electron, $\Phi_{Ki}(\vec{r}_1) = e^{i\vec{K}_i\cdot\vec{r}_1}$ and $\Phi_{Kf}(\vec{r}_1) = e^{i\vec{K}_f\cdot\vec{r}_1}$ are the initial and final states of the particle treated as plane waves, and $|\vec{r}_1-\vec{r}_2|$ is the separation between the ion and the atomic electron.

The doubly differential cross section in the center of mass system for a transition from the initially filled K-shell to the continuum with energy tranfer WZ_{2K}^2 Ry and momentum transfer $Z_{2K}Q^{1/2}/a_o$ is given by[3]

$$d^2\sigma_{WK} = 8\pi Z_1^2 \left(\frac{e^2}{\hbar v_1}\right)^2 \frac{dQ}{Q^2} \mid F_{WK}(Q) \mid^2 dW \frac{a_o^2}{Z_{2K}^2} \qquad \text{(II.2)}$$

using a hydrogenic model to describe the electron states by hydrogenic wave function; we have

$$\mid F_{WK}(Q) \mid^2 = \frac{1}{1-e^{-2\pi/k}} \times 2^7 Q \exp\{-(2/k)\arctan[2k/(Q-k^2+1)]\}$$

$$\times \frac{Q+\frac{1}{3}(k^2+1)}{[(Q-k^2+1)^2+4k^2]^3} \qquad \text{(II.3)}$$

where v_1 is the relative velocity between the projectile and target ($v_1=2E_1/M_1$), E_1 is the incident energy in the laboratory, M_1 is the projectile mass, Z_1e is the charge of the incident projectile, $k^2 = W-1$, a_o is the Bohr radius of hydrogen, $a_{2K}= a_o/Z_{2K}^2$, Ry denotes the Rydberg constant and $Z_{2K}e=(Z_2-0.3)e$ is a screened charge[36] for the target nucleus.

The differential cross section per interval of energy transfer can now be obtained by integrating Eq. (II.2) over the momentum transfer variable Q. The limits of the integration are established from conservation of energy. The assumption $\hbar\omega_{2K}/E_{CM}<<1$ is usually introduced in evaluating these limits. The limits are denoted by Q_{min} and Q_{max}.

The integration over Q yields the excitation function[3] $I_K(W)$, given by

$$I_K(W) = \int_{Q_{min}}^{Q_{max}} | F_{WK}(Q) |^2 \frac{dQ}{Q^2} \qquad \text{(II.4)}$$

The K-shell differential energy transfer cross section is now given by

$$d\sigma_K = 8\pi Z_1^2 a_0^2 Z_{2K}^{-4} \eta_K^{-1} I(W)dW \qquad \text{(II.5)}$$

where

$$\eta_K = (v_1/Z_{2K}v_o)^2 = \frac{m}{M_1}\frac{E_1}{Z_{2K}^2 Ry} \qquad \text{(II.6)}$$

and m is the electron mass, and $v_o = e^2/\hbar$. Eq. (II.5) can now be integrated to give the total direct Coulomb ionization cross section for the K-shell, σ_K.

$$\sigma_K = 8\pi Z_1^2 \, a_o^2 \, Z_{2K}^{-4} \, \eta_K^{-1} \int_{\theta_K}^{W_{max}} I_K(W)dW \qquad \text{(II.7)}$$

where θ_K corresponds to the minimum energy transferred, the actual ionization potential of the K-shell ($\hbar\omega_{2K}$), and is defined as

$$\theta_K = \hbar\omega_{2K}/(Z_{2K}^2 Ry). \qquad \text{(II.8)}$$

It may also be viewed as a screening number since it is the ratio of the observed ionization potential to the ideal ionization potential without outer screening, Z_{2K}^2 Ry. It has values between 0.5 and 1.0. The maximum energy transferred is denoted by W_{max}.

It is customary[6] to define

$$f_K(\eta_K, \theta_K) = \int_{\theta_K}^{W_{max}} I_K(W)dW \qquad \text{(II.9)}$$

and

$$\sigma_{oK} = 8\pi Z_1^2 \, a_o^2 \, Z_{2K}^{-4} \qquad \text{(II.10)}$$

and to express the total cross section as

$$\sigma_K = \sigma_{oK}\, \eta_K^{-1}\, f_K(\eta_K, \theta_K) \qquad \text{(II.11)}$$

It has been shown[14] that the cross sections exhibit a universal behavior when $\theta_K f_K/\eta_K$ is plotted as a function of the single variable η_K/θ_K^2 in the low velocity region. By defining

$$F_K(\eta_K/\theta_K^2) = (\theta_K/\eta_K) f_K(\eta_K, \theta_K) \qquad \text{(II.12)}$$

the total cross section can now be written as

$$\sigma_K = \sigma_{oK}\, \theta_K^{-1}\, F_K(\eta_K/\theta_K^2) \qquad \text{(II.13)}$$

Evaluation of the Limits of Integration

The energy conservation condition limits the momentum transfer variable q as follows[3]

$$(\hbar q_{min})^2 = 2M(\sqrt{E_{CM}} - \sqrt{E_{CM}-\varepsilon})^2 \qquad \text{(II.14)}$$

and

$$(\hbar q_{max})^2 = 2M(\sqrt{E_{CM}} + \sqrt{E_{CM}-\varepsilon})^2 \qquad \text{(II.15)}$$

where $\hbar q$ is the magnitude of the momentum transferred, ε is the energy transferred and M is the reduced mass of the projectile -

target system. Converting these expressions to the variables η_K, $W = \varepsilon/Z_{2K}^2$ Ry, and Q defined earlier, the following is obtained;

$$Q_{min} = \rho^2 \eta_K \left[1 - \sqrt{1-(W/\rho\eta_K)}\right]^2 \qquad \text{(II.16)}$$

and

$$Q_{max} = \rho^2 \eta_K \left[1 + \sqrt{1-(W/\rho\eta_K)}\right]^2 \qquad \text{(II.17)}$$

where $\rho = M/m$.

If $\varepsilon << E_1$, or equivalently if $\hbar\omega_{2K} << E_{CM}$ then Q_{min} can be written for all practical purposes[3] as

$$Q_{min} = W^2/4\eta_k \qquad \text{(II.18)}$$

Similarly Q_{max} can be set equal to infinity.

For the W integration, W_{max} can be set equal to $\rho\eta_K$ since the energy transferred cannot exceed the energy of the incident particle. However, for all practical purposes W_{max} can also be approximated accurately by infinity.[3]

Values of $f_K(\eta_K,\theta_K)$ calculated using the approximate limits of integration have been tabulated by Khandewal, Choi and Merzbacher.[6] Values of $F_K(\eta_K/\theta_K^2,\theta_K)$ have been published[27] for an extended range of η_K/θ_K^2 and θ_K values, also using the approximate limits of integration.

In the remainder of this work the notation PWBA(Ex) and PWBA(Ap) will be used to distinguish between calculations with exact and approximate limits, respectively.

The use of the exact limits introduces a dependence on the mass through the variable ρ and therefore cross sections cannot be tabulated easily. The cross section ratio PWBA(Ex)/PWBA(Ap) is plotted in Figure 1 for $\theta = 1.0$ and several values of η_K versus $\mu = \frac{\hbar\omega_{2K}}{E_{CM}}$. The upper scale gives the energy in MeV for protons incident on copper, where $\theta = 0.8$ and $0.005 \leq \eta_K < 0.5$. It should be noted that for small $\mu = \frac{\theta}{\rho\eta_K} = \hbar\omega_{2K}/E_{CM}$ the cross section ratio approaches unity. This is where the K-shell binding energy is much less than E_{CM} as required for the validity of the approximate limits. The ratio reaches approximately 0.75 for $\mu = 0.1$. Details of the actual numerical integration and tabulated values of the cross section ratios can be found elsewhere.[37]

Modifications to the PWBA

As mentioned earlier discrepancies between the PWBA and experimental data have been observed for low projectile velocities. Modifications to the basic theory have been suggested which account for increased binding of the target K-shell electron, polarization of the electron orbit due to distant ions, Coulomb deflection of the projectile from the straight line path implied in the PWBA and the relativistic electron velocities of higher Z_2 targets.

The first effect deals with the increased binding energy of the target electron. Since the slow ions have to penetrate the K-shell to cause ionization, the electrons become more tightly bound to the K-shell region, this effect is treated as a small perturbation to the electron binding energy as[14]

$$\epsilon\theta_K \equiv \epsilon_K(\xi_K)\theta_K = \left[1+2(Z_1/Z_{2K}\theta_K)g(\xi_K)\right]\theta_K \qquad \text{(II.19)}$$

where $\xi_K = 2n_K^{\frac{1}{2}}/\theta_K$ and $g(\xi_K)$ is obtained by numerical integration but is given within 1% by the analytic expression[14]

$$g(\xi_K) = (1+\xi_K)^{-5}\,(1+5\xi_K+7.14\xi_K^2+4.27\xi_K^3 + 9.47\xi_K^4) \qquad \text{(II.20)}$$

When the binding effect is included the cross section becomes

$$\sigma_K = (\sigma_{oK}/\epsilon\theta_K)F(\eta_K/(\epsilon_K\theta_K)^2 \qquad \text{(II.21)}$$

The second effect, polarization, becomes important for fast incident ions of charge Z_1e. Polarization effects have been studied from a classical approach[38] and a quantum mechanical approach.[39] These models treat the bound atomic electron as an isotropic harmonic oscillator. Only distant collisions or large impact parameters are considered in a multipole expansion in powers of the projectile target distance. The effect is incorporated along with the binding effect in the PWBA by modifying

the binding energy parameter θ_K by[32]

$$\zeta_K(\xi_K,c_K)\theta_K = \left[1+\frac{2Z_1}{\theta_K Z_{2K}}\{g(\xi_K,c_K) - h(\xi_K,c_K)\}\right]\theta_K \qquad \text{(II.22)}$$

where $g(\xi_K,c_K)$ is given by Eqs. (39) - (42) of Reference 32, and $h(\xi_K,c_K)$ is given by Eq. (27) of Reference 32. The parameter c_K is discussed in Reference 32. In Eq. (II.22) $g(\xi_K,c_K)$ represents the binding effect (increasing θ_K) and $h(\xi_K,c_K)$ represents the polarization effect (decreasing θ_K). The cross section which includes these effects has its origin in the PSS theory but for convenience is cast in terms of the PWBA with reduced variables giving

$$\sigma_K(\text{PSS}) = (\sigma_{oK}/\zeta_K\theta_K)F(\eta_K/(\zeta_K\theta_K)^2) \qquad \text{(II.23)}$$

In calculations used in this work the polarization effects are negligible but the PSS calculation was used for the sake of completeness in obtaining the "best" possible theoretical description available.

The Coulomb deflection of the incident projectile by the target nucleus was first treated by Bang and Hansteen[40] by first order time dependent scattering theory. An approximate Coulomb deflection factor was extracted by Brandt[14] *et al.* which was used to modify the PWBA to include Coulomb deflection. The PWBA modified to include Coulomb deflection is;

$$\sigma_K^{Coulomb} = 9E_{10}(\pi dq_o)\sigma_K \qquad (II.24)$$

where $0 \leq 9E_{10}(x) \leq 1$ for all $x \geq 0$. The function $E_{10}(x) = \int_1^\infty t^{-10} e^{-xt} dt$ is the exponential integral of order 10 and can be approximated by[41]

$$9E_{10}(x) = 9/(9+x)\ e^{-x} \qquad (II.25)$$

and $\pi dq_o = \frac{1}{2}\pi Z_1 (m/M)\theta_K^{-2}\ (\eta_K/\theta_K^2)^{-3/2}$ where $d = \frac{1}{2}(Z_1 Z_2 e^2/\frac{1}{2}Mv_1^2)$ is the half distance of closest approach in a head-on collision, and $q_o^{-1} = \hbar v_1/\hbar\omega_{2K}$ is the optimum penetration distance for K-shell ionization.[40] The approximate form of $E_{10}(\pi dq_o)$ used was checked throughout the range of πdq_o and was found to be adequate. Hereafter, this Coulomb deflection factor will be referred to as

$$C_B = 9E_{10}(\pi dq_o) \qquad (II.26)$$

Recently Kocbach[42] made a calculation using nonrelativistic electron wave functions and Rutherford trajectories. His results for the Coulomb deflection factor can be approximated by[31]

$$C_K = (.22+.78e^{1.9\pi dq_o})^{-1} \qquad (II.27)$$

The function C_K decreases much more rapidly than C_B in the low velocity region. Incorporation of the Coulomb deflection

effect with the theory which includes binding and polarization effects is accomplished by replacing θ_K with $\zeta_K\theta_K$. Thus, the perturbed stationary state theory with Coulomb deflection (CPSS) is given by

$$\sigma_K(\text{CPSS}) = C(\pi d\zeta_K q_o)\sigma_{oK}/(\zeta_K\theta_K)F(\eta_K/(\zeta_K\theta_K)^2) \qquad \text{(II.28)}$$

Here $C(\pi d\zeta_K q_o)$ represents either C_B or C_K as defined in Eq. (II.26) or (II.27), respectively.

Relativistic correction factors designed to compensate for the use of nonrelativistic electron wave functions have been calculated and published by many authors.[2,9,13,30,31] Anholt calculated ratios of PWBA cross sections using relativistic and nonrelativistic wave functions and derived a simple empirical formula to fit these calculations.[31] Defining $Q_A \equiv q_o a_K$, the relativistic correction factor is given by

$$R_A = \max(R_{BH}, R_{A'}) \qquad \text{(II.29)}$$

where $\max(R_{BH}, R_{A'})$ represents the maximum of R_{BH} and $R_{A'}$ which are defined by

$$R_{BH} = Q_A^{4(1-\gamma)}\left[1+(1-\gamma)\frac{\pi}{2}\left(\frac{3+2\gamma}{5+4\gamma}\right)Q_A\right]^2, \qquad \text{(II.30)}$$

$$R_{A'} = G(Z_F)Q_A^{4(1-\gamma_R)}\left[1+S(\gamma_R)(Q_A-Q_A^{-1}) - (1-\gamma_R)(1-(7/3)Q_A^{-2})\right]^2 \qquad \text{(II.31)}$$

$$S(\gamma) = \begin{cases} \tfrac{1}{2}\sin\gamma, & \gamma > 0.5 \\ \tfrac{1}{2}, & \gamma < 0.5 \end{cases}$$

$\gamma = (1-\alpha^2 Z_F^2)^{\frac{1}{2}}$, $\gamma_R = (1-\alpha^2 Z_R^2)^{\frac{1}{2}}$, and $G(Z_F)$ and Z_R are empirically determined functions of Z_F.[36] Normally $Z_F \equiv Z_2$.

Recently Brandt and Lapicki[43] have introduced a relativistic correction to the PWBA and PSS theories which is introduced by modifying the velocity dependent parameter η_K according to

$$\eta_K^R = \left[(1+\beta Y_K^2)^{\frac{1}{2}}+Y_K\right]\eta_K \qquad \text{(II.32)}$$

where $\beta = 1.1$ and $Y_K = 0.4(Z_{2K}/137)^2/\xi_K$. Theoretical calculations which include relativistic corrections will be denoted by the suffix R_A (Anholt) or R_B (Brandt).

CHAPTER III

EXPERIMENTAL PROCEDURE AND DATA ANALYSIS

The incident beams of protons, deuterons and $^{4}_{2}He^{+}$ ions were produced by the High Voltage Engineering Corporation 2.5 MV Van de Graaff Accelerator at the Regional Atomic and Nuclear Physics Laboratory at North Texas State University. The ion beams were energy and mass analyzed to an accuracy of 1% by a calibrated bending magnet. The analyzed beam was collimated by two 2 mm diameter tantalum apertures located approximately 75 cm before the target chamber and by a 3 mm diameter Carbon aperture at the entrance of the target chamber. The targets were mounted on a ladder which was rotated to position the targets at 45 degrees to the incident beam. The targets used ranged in thickness from 16 to 200 $\mu g/cm^2$. Some were self-supporting and others were mounted on 10-50 $\mu g/cm^2$ carbon backings. Measured target thicknesses are listed in Table 1. All target thicknesses were measured using Rutherford scattering with 1-2 MeV protons at an angle of 150 degrees. Calculated target thickness uncertainties are $\pm 7\%$. An ORTEC intrinsic Ge detector with a resolution of 225 eV FWHM at 5.9 KeV was positioned inside the target chamber approximately 2 cm from the target and at 90 degrees to the incident beam direction. A Si surface barrier detector was mounted at 150 degrees to the incident beam direction to detect the elastically scattered particles.

After passing through the target the incident particles were collected in a Faraday cup behind the chamber which was equipped with a -300 V electron suppressor to allow accurate current integration.

The Ge detector was calibrated for efficiency and solid angle using calibrated sources of ^{65}Zn, ^{155}Eu- and ^{241}Am by procedures described in the literature.[44] A 0.66 mm Mylar foil was placed between the target and the beryllium window of the detector to suppress low energy L-shell x-rays and to keep scattered particles from entering the x-ray detector.

The Si surface barrier detector was equipped with a 1 mm collimater to prevent high count rates from the large Rutherford scattering cross sections at low incident energies. The surface barrier detector had a FWHM resolution of 18 keV and was calibrated for efficiency and solid angle using a calibrated ^{244}Cm source.

The x-ray and elastically scattered particle spectra were stored in 1024 channels of both Tennecomp and Tracor Northern multichannel analyzers. Beam currents of up to 150 nanoamperes were obtained to keep dead time corrections to 2% or less. After background subtraction was performed, x-ray and scattered particle yields were extracted from the respective spectra.

Each target was bombarded by all three projectiles before being moved to insure that detector geometries and target thicknesses did not change from one projectile to the next. For each element data was taken for several different target thicknesses so that dependence on target thickness could be determined.

Experimental x-ray production cross sections were deduced from measured quantities via the following equation

$$\sigma_{Kexp} = \left(\frac{Y_{x\alpha}}{\varepsilon_{x\alpha}} + \frac{Y_{x\beta}}{\varepsilon_{x\beta}} \right) \sigma_R \frac{d\Omega_R}{Y_R} \left(1 - \frac{\overline{\Delta E}}{E_1}\right)^{-(s+2)} \frac{DTX}{DTR} \qquad \text{(III.1)}$$

where $Y_{x\alpha}$ = the measured K_α x-ray yield

$Y_{x\beta}$ = the measured K_β x-ray yield

$\varepsilon_{x\alpha}$ = the Ge detector efficiency for the K_α x ray

$\varepsilon_{x\beta}$ = the Ge detector efficiency for the K_β x ray

$\sigma_R = 1.296 \times 10^{-27} \left(\frac{Z_1 Z_2}{E_1(\text{MeV})} \right)^2 \frac{1}{\sin^4(\theta/2)} \frac{\text{cm}^2}{\text{sr}}$ = Rutherford scattering cross section

$d\Omega_R$ = solid angle subtended by the charged particle detector in sr.

Y_R = Measured yield of incident particles scattered from the target atom at angle θ

$\overline{\Delta E}$ = Average energy loss in passing through the target foil ($=\frac{1}{2} \frac{dE}{dX}.(\rho t)$)

E_1 = incident particle energy

DTX = dead time correction for x-ray yield

DTR = dead time correction for scattered particle yield

ρt = target thickness in $\mu g/cm^2$

dE/dX = stopping power for target element and incident projectile in $(\text{MeV} \cdot \text{cm}^2/\mu g)$[45]

s = slope of the cross section curve as a function of E_1 evaluated at E_1 using the theoretical predictions of the CPSSR.

It should be noted that $(1-\overline{\Delta E}/E)^{-(s+2)}$ is a correction to the x-ray and Rutherford yields to compensate for the energy loss in the target.[46] Because of the large slope of the x-ray cross section as a function of energy in the region studied ($3<s<7$) and the large energy losses encountered for low energy ions passing through the thickest foils ($\overline{\Delta E}/E \leq .075$), values of this correction factor were as large as a factor of 2. To test its validity, cross section measurements made for several different target thicknesses at the same incident energy and corrected according to Eq. (III.1) were found to agree well within experimental uncertainties.

Sources of experimental uncertainty are tabulated in Table 2. The largest uncertainty in the x-ray cross section derives from the strong energy dependence of the cross section

$$Y \alpha \sigma_x \alpha E_1^s$$

so,

$$\frac{dY}{Y} = s\frac{dE_1}{E_1} \qquad \text{(III.2)}$$

where dE_1/E_1 is the uncertainty in the incident projectile energy. Thus, with s as large as 7 and $dE_1/E_1 = 0.01$, uncertainties of 7% in the measured x-ray yield for incident energy E_1 could be introduced. Due to lack of calibration points for the magnet system in the low energy region (<0.16 MeV) this

uncertainty may be even larger for the lowest values of E_1 due to the extrapolation of the energy calibration into this region (expect $dE_1/E_1 < 0.02$ at 0.1 MeV).

CHAPTER IV

DISCUSSION OF RESULTS

The measured K-shell x-ray production cross sections for incident protons, deuterons and alpha particles are presented in Tables 3 to 5, respectively. Also tabulated are calculated values of the PSS theory with Coulomb deflection effects (C_K and C_B) and relativistic effects (R_A and R_B). These theoretical values have been converted from ionization to x-ray production cross sections using the fluorescence yield values (ω_K) of Bambynek et al.[47] The fluorescence yields used are for single vacancies and should be valid for all experimental work presented here.

It was noted earlier that the difference between the theoretical calculations of ionization cross sections with exact and approximate limits reaches about 25-30% for the lowest incident energies measured. Figure 2 shows these two calculations for protons incident on $_{29}$Cu along with the measured absolute values of this work and others.[33,34,48] The agreement between this work and that of Reference 34 is well within experimental uncertainties. Cross section values from the other studies are higher than the present ones by more than experimental uncertainties. Experimental values for the other projectile-target combinations agree with the published values of Reference 29,

but are generally higher than those in Reference 33 and 34 for protons and alphas on $_{47}Ag$ by as much as 50%.

The theoretical curves in Figure 2 include the Coulomb deflection factor of Brandt et al.[14] (C_B) but do not contain any correction for relativistic effects. It is evident that the use of the exact limits does not account for the difference in energy dependence between theory and experiment. The inclusion of relativistic effects will raise both the predictions of the theories above the experimental data at the lowest energies and improve the agreement at the higher energies. The data for protons on other target elements show similar tendencies. The difference between the calculations with exact and approximate limits is smaller for the heavier projectiles at the same velocity but the relationships between theory and experiment are similar.

Figures 3 to 6 show comparisons between theoretical and experimental values of absolute x-ray production cross sections for all three projectiles and all four target elements used. Theoretical calculations employ the exact limits of integration. The four different theoretical calculations represent the PSS including combinations of the two Coulomb deflection calculations (C_K and C_B) and the two relativistic corrections (R_A and R_B) discussed earlier.

The effect of the two relativistic calculations are almost identical; Anholt's calculation gives slightly lower values at the lowest energies, with the difference being larger for higher Z_2 and larger Z_1. The largest difference between the relativistic treatments is ~20% for ^4_2He on $_{51}Sb$ at 0.2 MeV/amu.

The two calculations for the Coulomb deflection effects are quite different. Although they converge at the highest energies for $^{4}_{2}He + {}_{29}Cu$, the difference grows for the lighter projectiles and heavier targets at lower energies. Kocbach's calculation is always lower and decreases much more rapidly at lower energies than the calculation of Brandt et al.[14] The two calculations differ by a factor of ∿6 for $^{1}_{1}H$ on $_{29}Cu$ at 0.1 MeV/amu.

In general, the experimental data do not agree with the energy dependence of any of the four theoretical predictions. The majority of the absolute data agree with the $C_B PSSR$ (here $R = R_A$ or R_B since they are identical) from the highest energies down to the middle of the energy range within experimental uncertainties. At this point the data decreases more rapidly than the $C_B PSSR_A$ and reaches the predictions of the $C_K PSSR_B$ at the lowest incident energies. With the exception of the $_{41}Nb$ data, this tendency is present for all three projectiles and all four targets. For $_{41}Nb$ the experimental data seems high relative to the theoretical predictions but exhibits the same relative energy dependence.

Since the effect of the exact versus approximate limits is small compared to discrepancies between theory and experiment, and since the numerical difference between the two relativistic treatments is also relatively small, it is reasonable to examine the two Coulomb deflection calculations more closely. An experimental Coulomb deflection factor can be derived by dividing

the experimental cross section by the theoretical prediction of the PSSR. If the theoretical calculation accurately accounts for binding, polarization (negligible here) and relativistic effects, the data are an experimental measure of $C(\pi dq_o)$. Figure 7 shows the plot of these data for all projectiles and targets versus the Coulomb deflection variable πdq_o). The data exhibit universal behavior although the spread in the data is considerably larger than the experimental uncertainties. The locus of the data points is a line on the semi-log plot which crosses $C_B(\pi dq_o)$ at $\pi dq_o = 0.5$ and has a slope close to that of $C_K(\pi dq_o)$ but is displaced from it by a factor of ~ 2.5 at $\pi dq_o = 2.5$ and ~ 1.3 at $\pi dq_o = 0.5$.

To investigate further the Coulomb deflection effect, ratios of cross sections for x-ray production induced by deuterons to those induced by protons were calculated, and are plotted in Fig. 8. The targets are the same for each projectile. Since ${}^2_1D$ and ${}^1_1H$ have the same Z_1 but different charge to mass ratios, the increased binding effect is the same for both while the Coulomb deflection is not. In addition, experimental normalization factors cancel so that the ratio of measured cross sections are more certain than the cross sections themselves. The difference between calculations made with exact and approximate limits is smaller than experimental uncertainties. The ratios of experimental data fall between the predictions of the C_KPSS(Ex) and the C_BPSS(Ex) as in the case of absolute cross sections. The experimental ratio values differ from the theoretical pre-

dictions by as much as a factor of 2 at the lowest energies while good agreement with the C_BPSS is found at the highest energies. Relativistic effects are not included because the calculations give the same result for projectiles at the same velocity bombarding the same target.

The ratio of cross sections for $^4_2$He and $^2_1$D projectiles at the same velocity bombarding the same target shows the velocity dependence and relative magnitude of the increased binding effect. The ratio is divided by four to take into account the Z_1^2 dependence given in the PWBA. Since $^4_2$He and $^2_1$D have the same charge to mass ratio the Coulomb deflection effect is the same for both except for the Z_1 dependence introduced through the variable ξ_K in the argument of the Coulomb deflection factor. Figure 9 shows both measured and theoretical values of this ratio for $_{29}$Cu and $_{47}$Ag. The agreement between theory and experiment is quite good and usually within experimental uncertainties. The theoretical ratio values calculated with approximate limits deviate from those calculated with exact limits by less than experimental uncertainties.

The velocity dependence of theoretical models can be tested most easily by comparing relative cross section values. To do so, the measured values of the cross sections for each projectile-target combination are normalized to the measured value of the cross section at the largest velocity.

$$\sigma^{Exp}_{relative}(V_1) = \sigma^{Exp}_{Kx}(V_1)/\sigma^{Exp}_{Kx}(V_{max}) \qquad \text{(IV.1)}$$

Similarly, the theoretical values are normalized to the theoretical value at the largest velocity.

$$\sigma^{\text{Theor}}_{\text{relative}}(v_1) = \sigma^{\text{Theor}}(v_1)/\sigma^{\text{Theor}}(v_{max}). \qquad \text{(IV.2)}$$

Figure 10 is a plot of ratios of measured cross section values normalized in this way to theoretical cross section values normalized in this way. The deviation of these ratios from unity is a measure of the difference in the velocity dependence of the measured and theoretical values for the cross sections. The two theoretical calculations used give the best agreement with results of experiment. The plotted ratio values which are greater than unity indicate that the theoretical prediction decreases more rapidly as a function of decreasing velocity than the measured values. Ratio values below unity indicate that the measured values for the cross sections decrease more rapidly with decreasing velocity than the theoretical predictions.

The plotted ratios for protons on $_{29}Cu$ show that the relative values of the $C_K PSSR_B$ underpredict the relative values of the measured cross sections by almost a factor of three at the lowest energies. This discrepancy in the velocity dependence between the $C_K PSSR_B$ and the measured values decreases systematically with increasing Z_2 and the ratio values for protons on $_{51}Sb$ are within 20% of unity for all velocities. For alpha particles, however, the Z_2 dependence of the ratios is reversed with the best agreement for $_{29}Cu$ and the worst for $_{51}Sb$. For deuterons there is no obvious Z_2 dependence in the ratios and

the deviation from unity is $\pm 40\%$ for $_{41}Nb$ and $\pm 20\%$ for the other elements.

The relative values of the $C_B PSSR_A$ overpredict the relative measured values of the cross sections for protons on $_{47}Ag$ and $_{51}Sb$ by a factor of ~ 2.5 at the lowest velocities. This deviation of the ratios from unity decreases with decreasing Z_2 and the velocity dependence of the measured cross sections for protons on $_{29}Cu$ is predicted by the $C_B PSSR_A$ within 20%. For alpha particles and deuterons the Z_2 dependence of the deviation of the ratios from unity is reversed. The agreement is not nearly as good as it is for protons at the lowest velocities.

To summarize Figure 10, the deviation from unity of the ratios of relative measured values of the cross sections to relative theoretical values shows the inadequacy of either theoretical model to predict accurately the velocity dependence of the experimental data.

CHAPTER V

CONCLUSIONS

The primary purpose of this work was to determine the magnitude of the effect of the approximation $\hbar\omega_{2K}/E_{CM}<<1$, which is used in calculating ionization cross sections in the PWBA and PSS theories. Calculations without this approximation give values for the ionization cross sections which are lower by $\sim$25% at $\hbar\omega_{2K}/E_{CM} = 0.1$, than values from calculations in which the approximation is used. Avoiding this approximation also introduces a threshold effect which forces the ionization cross section to zero when $E_{CM}<\hbar\omega_{2K}$. Experiments designed to explore the low velocity dependence of ionization cross sections for signs of this threshold effect were carried out using three different projectiles (^1_1H, ^2_1D, ^4_2He). This permitted an examination of the data through the formation of cross section ratios whose values are free of the uncertainties of the various normalization factors which determine absolute cross sections. As a result, an assessment of the theory could be made more sensitively than by a simple comparison of absolute cross sections. Discrepancies much larger than the 25% effect of the approximation were found between theory and experiment in both the magnitude and energy dependence of the absolute cross sections. At these energies, the threshold effect is apparently too small to be seen.

Since both relativistic and Coulomb deflection effects are very large in this energy region, comparisons were also made with two different calculations of each of these effects. The two relativistic calculations give similar results, but the Coulomb deflection factors are quite different in both magnitude and energy dependence. In the ratio $\sigma(^{2}_{1}D)/\sigma(^{1}_{1}H)$ where relativistic and increased binding effects cancel, leaving only the Coulomb deflection effect, neither theory provides an adequate description of the experimental data. A measurement of the Coulomb deflection effect, derived using the theoretical predictions for both increased binding and relativistic effects, shows the same disagreement with both Coulomb deflection factors. This suggests that the theoretical predictions for the binding and relativistic effects are at least adequate in both magnitude and energy dependence. The ratio $\sigma(^{4}_{2}He)/4\sigma(^{2}_{1}D)$ which tests only the binding effect shows good agreement with theoretical predictions.

CHAPTER VI

SYMBOLS AND DEFINITIONS

a_o - Bohr radius of hydrogen = 0.529×10^{-8} cm

E_1 - Energy of incident particle in laboratory system

E_{CM} - Energy of incident particle in center of mass system

$f_k(\eta_K, \theta K)$ - Dimensionless integral proportional to cross section defined in Eq. (II.9)

$F_K(\eta_K/\theta^2, \theta)$ - Tabulated universal function = $\theta f_K/\eta_K$

$\hbar\omega_{2K}$ - Observed binding energy of K-shell

$I_K(W)$ - Excitation function, Eq. (II.4)

m - Electron mass

M_1 - Mass of incident particle

M - Reduced mass of projectile - target system

Q - (Momentum transfer)$^2 \times a_o^2/(Z_{2K}^2\hbar^2)$

Ry - Rydberg = 13.6eV

W - (Energy transferred to ejected electron)$/(Z_{2K}^2 Ry)$

$Z_1 e$ - Charge of projectile

$Z_{2K}e$ - Screened nuclear charge as seen by electron in K-shell ($Z_{2K}=Z_2-0.3$)

η_K - $(v_1/Z_{2K}v_o)^2 = mE_1/(M_1 Z_{2K}^2 Ry)$

v_o - Bohr velocity = $e^2/\hbar$

v_1 - Velocity of incident projectile in laboratory system

θ_K - K-shell screening number = $\hbar\omega_{2K}/(Z_{2K}^2 Ry)$

ϵ - Factor multiplied by θ_K to include increased binding effect

ζ - Factor multiplied by θ_K to include increased binding and polarization effects

TABLE I

TARGET THICKNESSES

Element	Z_2	Thickness* ($\mu g/cm^2$)
Cu	29	47.1 68.3 155.0 (SS)**
Nb	41	16.5 25.3 58.7
Ag	47	82.0 (SS) 131.0 (SS) 152.0 (SS)
Sb	51	61.2 207.0

* The target thicknesses given were measured with the target positioned in the beam at an angle of 45^{o} with respect to the incident beam direction.

** (SS) indicates self-supporting targets, all others were mounted on 10-50 $\mu g/cm^2$ carbon foils.

TABLE II

EXPERIMENTAL UNCERTAINTIES

Source	Range
Relative Uncertainty	
Counting Statistics and Background Subtraction	
K_α and K_β X-Ray Yields	1-4%
Back-Scattered Particle Yields	1-4%
Uncertainty in X-Ray Yield Due to Uncertainty in Incident Energy*	3-7%
Total Relative Uncertainty.....	<9%
Normalization Uncertainty	
Absolute Efficiency Calibration	
Source Strength	3%
Source X-Ray Yields	1-2%
Source Relative Photon Intensities	3%
Particle Detector Solid Angle	5%
Rutherford Differential Cross Section due to Uncertainty in Angle θ	5%
Total Normalization Uncertainty.....	<8.5%
TOTAL ABSOLUTE UNCERTAINTY	<12.4%

*This assumes a 1% uncertainty in the incident energy.

TABLE III

CROSS SECTIONS FOR K-SHELL X-RAY PRODUCTION BY PROTONS

(All Cross Sections are in Barns)*

E_1/M_1 (MeV/amu)	σ_x (Measured)	σ_x $C_B PSSR_A$	σ_x $C_K PSSR_A$	σ_x $C_B PSSR_B$	σ_x $C_K PSSR_B$
		Copper (Z_2=29, ω_K=0.445)			
0.1	1.37(-4)	2.15(-4)	4.65(-5)	2.25(-4)	4.87(-5)
0.12	5.92(-4)	7.95(-4)	2.63(-4)	8.20(-4)	2.71(-4)
0.14	1.69(-3)	2.14(-3)	9.26(-4)	2.18(-3)	9.43(-4)
0.16	3.82(-3)	4.65(-3)	2.41(-3)	4.72(-3)	2.45(-3)
0.18	7.60(-3)	8.87(-3)	5.24(-3)	9.00(-3)	5.32(-3)
0.20	1.33(-2)	1.53(-2)	9.92(-3)	1.49(-2)	9.66(-3)
0.25	3.91(-2)	4.47(-2)	3.35(-2)	4.44(-2)	3.33(-2)
0.30	8.48(-2)	1.00(-1)	8.14(-2)	1.01(-1)	8.22(-2)
		Niobium (Z_2=41, ω_K=0.748)			
0.2	7.07(-5)	9.72(-5)	2.00(-5)	1.07(-4)	2.20(-5)
0.24	3.15(-4)	3.56(-4)	1.13(-4)	3.81(-4)	1.21(-4)
0.28	9.61(-4)	9.43(-4)	3.96(-4)	1.02(-3)	4.28(-4)
0.32	2.14(-3)	2.05(-3)	1.04(-3)	2.14(-3)	1.09(-3)
0.36	4.28(-3)	3.87(-3)	2.24(-3)	3.87(-3)	2.24(-3)
0.40	7.65(-3)	6.61(-3)	4.21(-3)	6.61(-3)	4.21(-3)
0.45	1.39(-2)	1.17(-2)	8.15(-3)	1.15(-2)	8.01(-3)
0.50	2.32(-2)	1.89(-2)	1.40(-2)	1.84(-2)	1.36(-2)

*The notation 1.37(-4) denotes 1.37×10^{-4}

TABLE III (CONTD.)

E_1/M_1 (MeV/amu)	σ_x (Measured)	σ_x $C_B PSSR_A$	σ_x $C_K PSSR_A$	σ_x $C_B PSSR_B$	σ_x $C_K PSSR_B$
		Silver (Z_2=47, ω_K=0.83)			
0.25	1.96(-5)	4.61(-5)	7.96(-6)	5.34(-5)	9.22(-6)
0.30	1.16(-4)	1.76(-4)	4.92(-5)	1.96(-4)	5.48(-5)
0.35	3.75(-4)	4.83(-4)	1.84(-4)	5.33(-4)	2.03(-4)
0.40	1.00(-3)	1.06(-3)	4.96(-4)	1.14(-3)	5.33(-4)
0.45	2.01(-3)	2.03(-3)	1.10(-3)	2.10(-3)	1.14(-3)
0.50	3.64(-3)	3.52(-3)	2.13(-3)	3.40(-3)	2.06(-3)
0.55	6.08(-3)	5.61(-3)	3.68(-3)	5.56(-3)	3.65(-3)
0.60	9.57(-3)	8.48(-3)	5.92(-3)	8.36(-3)	5.84(-3)
		Antimony (Z_2=51, ω_K=0.867)			
0.30	1.86(-5)	4.33(-5)	7.77(-6)	5.15(-5)	9.24(-6)
0.35	7.25(-5)	1.33(-4)	3.58(-5)	1.52(-4)	4.09(-5)
0.40	2.03(-4)	3.22(-4)	1.15(-4)	3.64(-4)	1.30(-4)
0.45	5.49(-4)	6.54(-4)	2.84(-4)	7.22(-4)	3.14(-4)
0.50	1.12(-3)	1.18(-3)	5.93(-4)	1.27(-3)	6.38(-4)
0.55	1.82(-3)	1.97(-3)	1.11(-3)	2.00(-3)	1.13(-3)
0.60	3.00(-3)	3.06(-3)	1.87(-3)	3.06(-3)	1.87(-3)
0.65	4.77(-3)	4.51(-3)	2.95(-3)	4.47(-3)	2.92(-3)

TABLE IV

CROSS SECTIONS FOR K-SHELL X-RAY PRODUCTION BY DEUTERONS

(All Cross Sections are in Barns)*

E_1/M_1 (MeV/amu)	σ_x (Measured)	σ_x $C_B PSSR_A$	σ_x $C_K PSSR_A$	σ_x $C_B PSSR_B$	σ_x $C_K PSSR_B$
		Copper (Z_2=29, ω_k=0.445)			
0.08	6.90(-5)	2.11(-4)	7.60(-5)	2.24(-4)	8.07(-5)
0.09	2.25(-4)	4.43(-4)	1.89(-4)	4.66(-4)	2.02(-4)
0.10	6.09(-4)	8.24(-4)	4.18(-4)	8.60(-4)	4.36(-4)
0.12	2.03(-3)	2.23(-3)	1.37(-3)	2.29(-3)	1.41(-3)
0.14	4.59(-3)	4.86(-3)	3.38(-3)	4.96(-3)	3.45(-3)
0.16	9.18(-3)	9.21(-3)	6.93(-3)	9.34(-3)	7.03(-3)
0.18	1.63(-2)	1.57(-2)	1.25(-2)	1.60(-2)	1.27(-2)
0.20	2.58(-2)	2.51(-2)	2.08(-2)	2.45(-2)	2.03(-2)
0.25	6.59(-2)	6.40(-2)	5.63(-2)	6.35(-2)	5.59(-2)
0.30	1.45(-1)	1.33(-1)	1.21(-1)	1.34(-1)	1.22(-1)
		Niobium (Z_2=41, ω_K=0.748)			
0.16	5.09(-5)	1.02(-4)	3.57(-5)	1.17(-4)	4.10(-5)
0.20	4.63(-4)	3.88(-4)	1.93(-4)	4.27(-4)	2.12(-4)
0.24	1.35(-3)	1.03(-3)	6.25(-4)	1.10(-3)	6.67(-4)
0.28	3.02(-3)	2.22(-3)	1.53(-3)	2.39(-3)	1.65(-3)
0.32	5.60(-3)	4.14(-3)	3.09(-3)	4.31(-3)	3.22(-3)
0.36	1.03(-2)	7.00(-3)	5.53(-3)	7.00(-3)	5.53(-3)
0.40	1.52(-2)	1.10(-2)	9.04(-3)	1.10(-2)	9.04(-3)
0.45	2.35(-2)	1.80(-2)	1.54(-2)	1.77(-2)	1.51(-2)

*The notation 6.90(-5) denotes 6.90×10^{-5}

TABLE IV (CONTD.)

E_1/M_1 (MeV/amu)	σ_x (Measured)	σ_x $C_B PSSR_A$	σ_x $C_K PSSR_A$	σ_x $C_B PSSR_B$	σ_x $C_B PSSR_B$
		Silver (Z_2=47, ω_K=0.830)			
0.20	3.06(-5)	5.37(-5)	1.67(-5)	6.51(-5)	2.03(-5)
0.25	1.82(-4)	2.09(-4)	9.59(-5)	2.42(-4)	1.11(-4)
0.30	5.26(-4)	5.65(-4)	3.24(-4)	6.28(-4)	3.60(-4)
0.35	1.33(-3)	1.22(-3)	8.02(-4)	1.35(-3)	8.87(-4)
0.40	2.59(-3)	2.29(-3)	1.65(-3)	2.45(-3)	1.77(-3)
0.45	4.66(-3)	3.89(-3)	2.99(-3)	4.04(-3)	3.11(-3)
0.50	6.64(-3)	6.34(-3)	4.93(-3)	6.04(-3)	4.86(-3)
0.55	1.09(-2)	9.13(-3)	7.53(-3)	9.05(-3)	7.53(-3)
0.60	1.64(-2)	1.30(-2)	1.09(-2)	1.28(-2)	1.09(-2)
		Antimony (Z_2=51, ω_K=0.867)			
0.25	3.61(-5)	6.48(-5)	2.25(-5)	8.07(-5)	2.80(-5)
0.30	1.36(-4)	1.91(-4)	8.93(-5)	2.27(-4)	1.06(-4)
0.35	3.40(-4)	4.37(-4)	2.47(-4)	4.98(-4)	2.81(-4)
0.40	6.68(-4)	8.57(-4)	5.48(-4)	9.71(-4)	6.21(-4)
0.45	1.30(-3)	1.50(-3)	1.05(-3)	1.65(-3)	1.16(-3)
0.50	2.24(-3)	2.42(-3)	1.80(-3)	2.59(-3)	1.93(-3)
0.55	3.57(-3)	3.66(-3)	2.85(-3)	3.71(-3)	2.89(-3)
0.60	5.35(-3)	5.30(-3)	4.29(-3)	5.30(-3)	4.29(-3)
0.65	6.76(-3)	7.38(-3)	6.28(-3)	7.31(-3)	6.22(-3)

TABLE V

ALPHA-PARTICLE INDUCED TOTAL K-SHELL X-RAY PRODUCTION CROSS SECTIONS

(All Cross Sections are in Barns)*

E_1/M_1 (MeV/amu)	σ_x (Measured)	σ_x $C_B PSSR_A$	σ_x $C_K PSSR_A$	σ_x $C_B PSSR_B$	σ_x $C_K PSSR_B$
		Copper (Z_2=29, ω_K=0.445)			
0.08	1.58(-4)	4.11(-4)	1.31(-4)	4.55(-4)	1.45(-4)
0.09	5.83(-4)	8.57(-4)	3.31(-4)	9.38(-4)	3.65(-4)
0.10	1.12(-3)	1.67(-3)	7.79(-4)	1.81(-3)	8.44(-4)
0.12	3.92(-3)	4.69(-3)	2.72(-3)	4.99(-3)	2.89(-3)
0.14	9.99(-3)	1.05(-2)	6.98(-3)	1.10(-2)	7.31(-3)
0.16	2.07(-2)	2.02(-2)	1.47(-2)	2.10(-2)	1.53(-2)
0.18	3.69(-2)	3.51(-2)	2.72(-2)	3.71(-2)	2.87(-2)
0.20	5.81(-2)	5.67(-2)	4.59(-2)	5.70(-2)	4.61(-2)
0.25	1.42(-1)	1.49(-1)	1.29(-1)	1.52(-1)	1.32(-1)
0.30	2.73(-1)	3.16(-1)	2.87(-1)	3.14(-1)	2.85(-1)
		Niobium (Z_2=41, ω_K=0.748)			
0.16	1.40(-4)	2.49(-4)	7.93(-5)	2.99(-4)	9.52(-5)
0.20	1.14(-3)	9.67(-4)	4.51(-4)	1.12(-3)	5.22(-4)
0.24	2.97(-3)	2.62(-3)	1.52(-3)	2.93(-3)	1.70(-3)
0.28	7.37(-3)	5.71(-3)	3.79(-3)	6.23(-3)	4.14(-3)
0.32	1.44(-2)	1.08(-2)	7.84(-3)	1.21(-2)	8.78(-3)
0.36	2.57(-2)	1.84(-2)	1.42(-2)	1.96(-2)	1.51(-2)
0.40	4.04(-2)	2.93(-2)	2.37(-2)	3.00(-2)	2.43(-2)
0.45	7.02(-2)	4.82(-2)	4.06(-2)	4.91(-2)	4.14(-2)

*The notation 1.58(-4) denotes 1.58×10^{-4}

TABLE V (CONTD.)

E_1/M_1 (MeV/amu)	σ_x (Measured)	σ_x $C_B PSSR_A$	σ_x $C_K PSSR_A$	σ_x $C_B PSSR_B$	σ_x $C_K PSSR_B$
		Silver (Z_2=47, ω_K=0.830)			
0.15	4.56(-6)	1.71(-5)	2.16(-6)	2.34(-5)	2.96(-6)
0.20	1.10(-4)	1.41(-4)	4.02(-5)	1.81(-4)	5.16(-5)
0.25	5.10(-4)	5.76(-4)	2.49(-4)	6.85(-4)	2.92(-4)
0.30	1.55(-3)	1.58(-3)	8.66(-4)	1.79(-3)	9.81(-4)
0.35	3.68(-3)	3.46(-3)	2.20(-3)	3.80(-3)	2.42(-3)
0.40	6.73(-3)	6.52(-3)	4.58(-3)	7.32(-3)	5.14(-3)
0.45	1.27(-2)	1.12(-2)	8.43(-3)	1.18(-2)	8.88(-3)
0.50	2.00(-2)	1.77(-2)	1.40(-2)	1.81(-2)	1.43(-2)
0.55	3.14(-2)	2.58(-2)	2.12(-2)	2.63(-2)	2.16(-2)
0.60	4.63(-2)	3.79(-2)	3.20(-2)	3.76(-2)	3.17(-2)
		Antimony (Z_2=51, ω_K=0.867)			
0.20	2.03(-5)	3.96(-5)	7.40(-6)	5.57(-5)	1.04(-5)
0.25	1.38(-4)	1.78(-4)	5.73(-5)	2.38(-4)	7.66(-5)
0.30	4.46(-4)	5.30(-4)	2.35(-4)	6.69(-4)	2.97(-4)
0.35	1.18(-3)	1.24(-3)	6.72(-4)	1.49(-3)	8.07(-4)
0.40	2.50(-3)	2.43(-3)	1.50(-3)	2.83(-3)	1.75(-3)
0.45	4.85(-3)	4.29(-3)	2.92(-3)	5.06(-3)	3.44(-3)
0.50	7.59(-3)	6.96(-3)	5.07(-3)	7.84(-3)	5.71(-3)
0.55	1.17(-2)	1.06(-2)	8.12(-3)	1.18(-2)	9.04(-3)
0.60	1.70(-2)	1.54(-2)	1.23(-2)	1.59(-2)	1.27(-2)

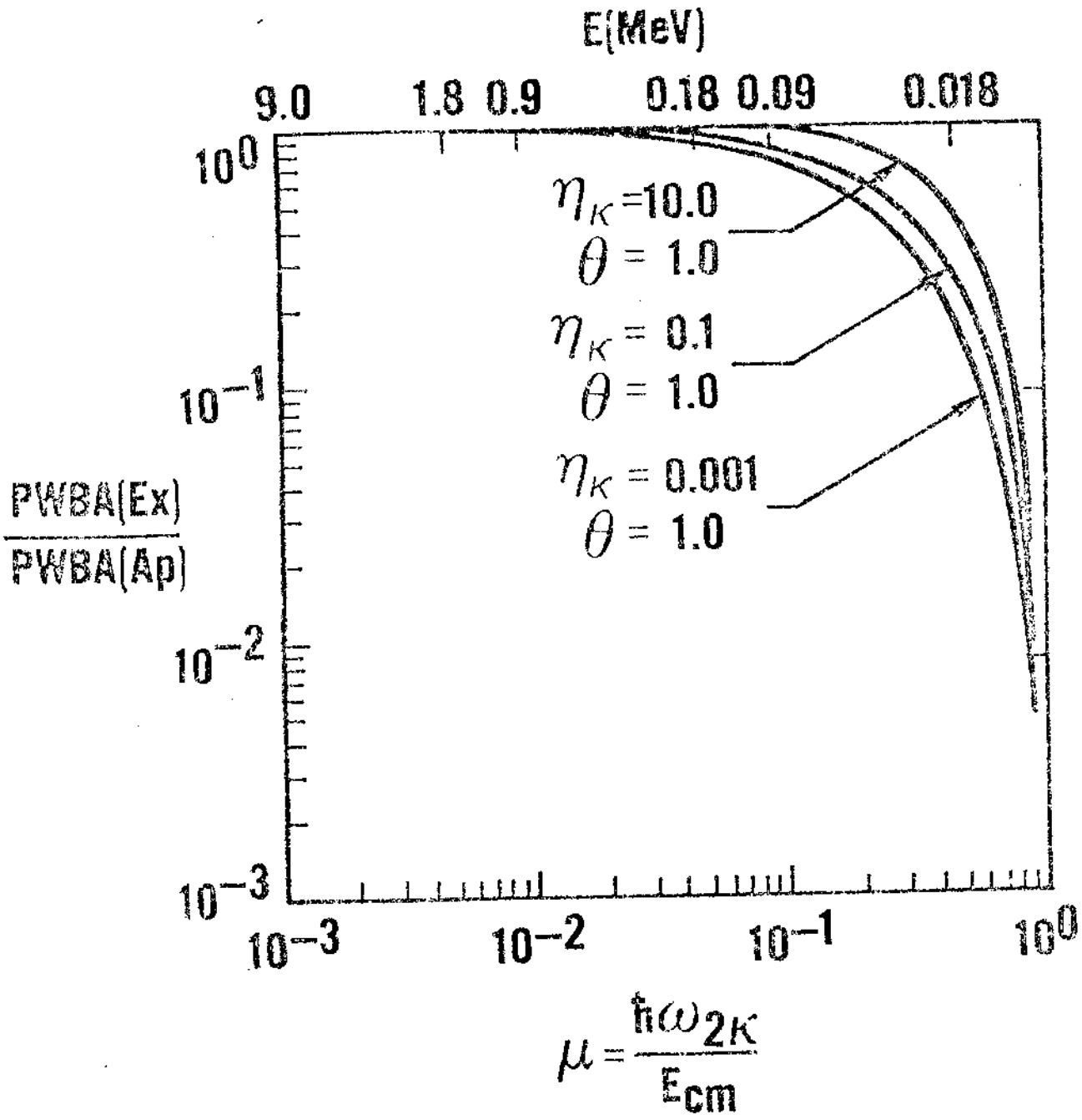

Fig. 1--Ratio of PWBA(Ex) to PWBA(Ap) for θ=1.0 and η_K=0.001, 0.1, and 10.0 versus $\mu=\hbar\omega_{2K}/E_{CM}$.

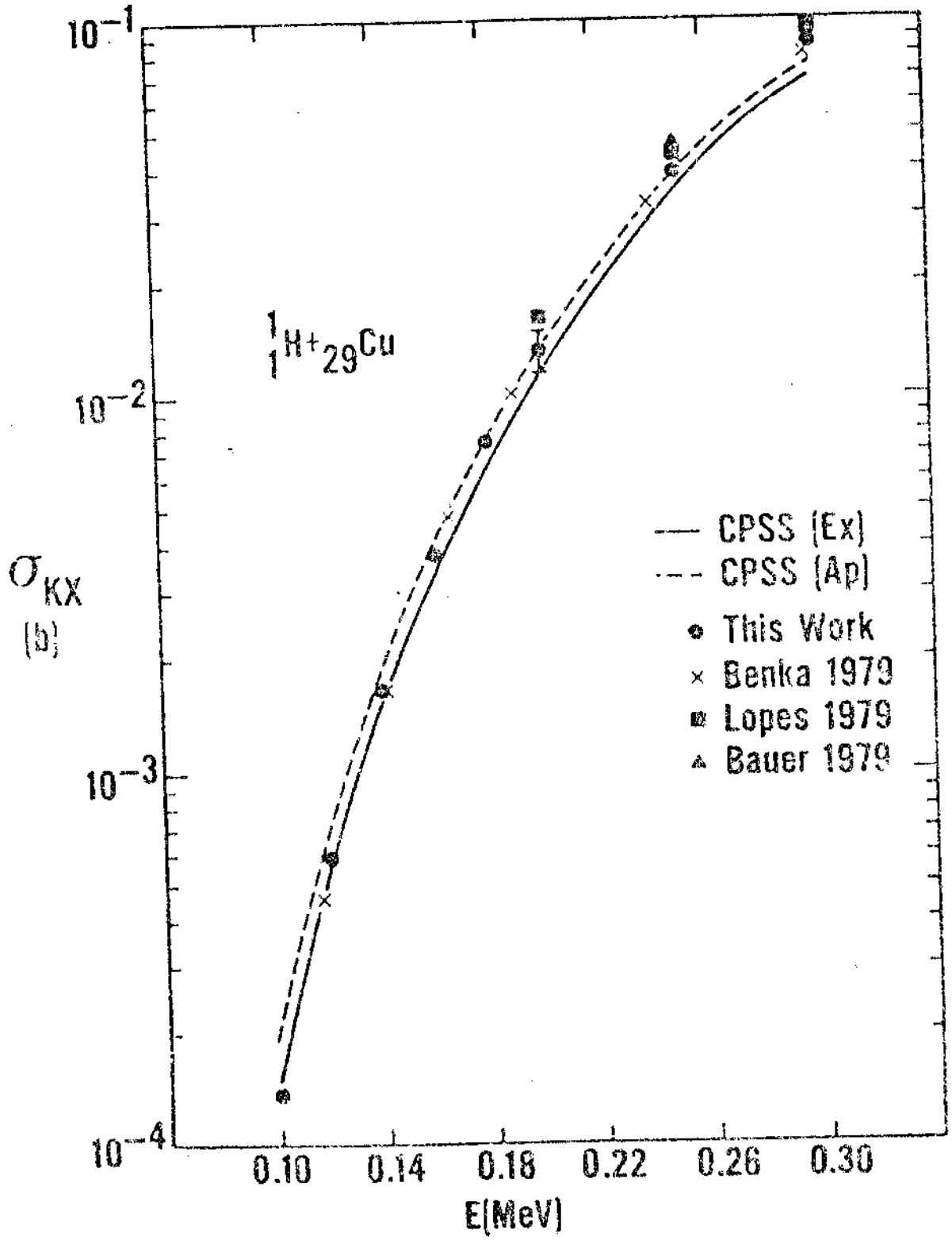

Fig. 2--K-Shell X-Ray Production Cross Sections for Protons on $_{29}Cu$.

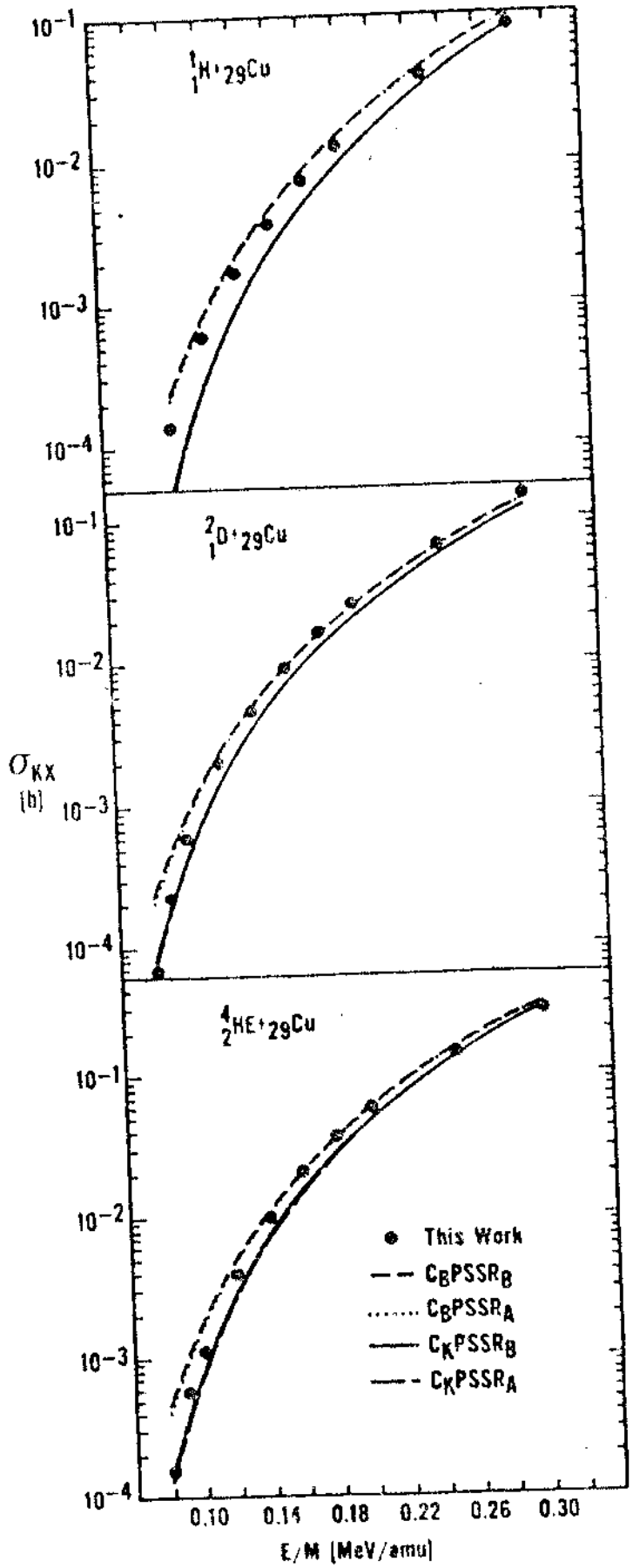

Fig. 3--Measured K-Shell X-Ray Production Cross Sections Compared to Theoretical Predictions of the $C_K PSSR_A$, $C_K PSSR_B$, $C_B PSSR_A$, and $C_B PSSR_B$ for $^{1}_{1}H$, $^{2}_{1}D$, and $^{4}_{2}He$ Ions Incident on $_{29}Cu$.

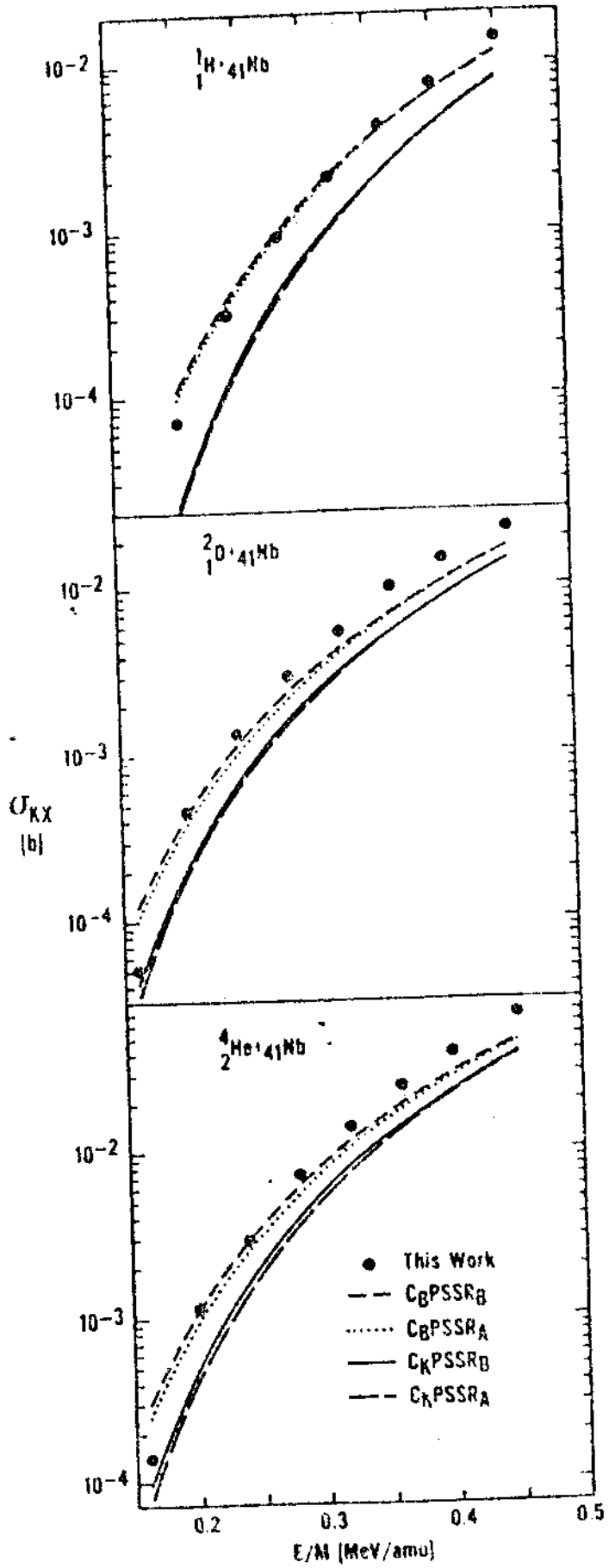

Fig. 4--Measured K-Shell X-Ray Production Cross Sections Compared to Theoretical Predictions of the $C_K PSSR_A$, $C_K PSSR_B$, $C_B PSSR_A$, and $C_B PSSR_B$ for $^{1}_{1}H$, $^{2}_{1}D$, and $^{4}_{2}He$ Ions Incident on ^{41}Nb.

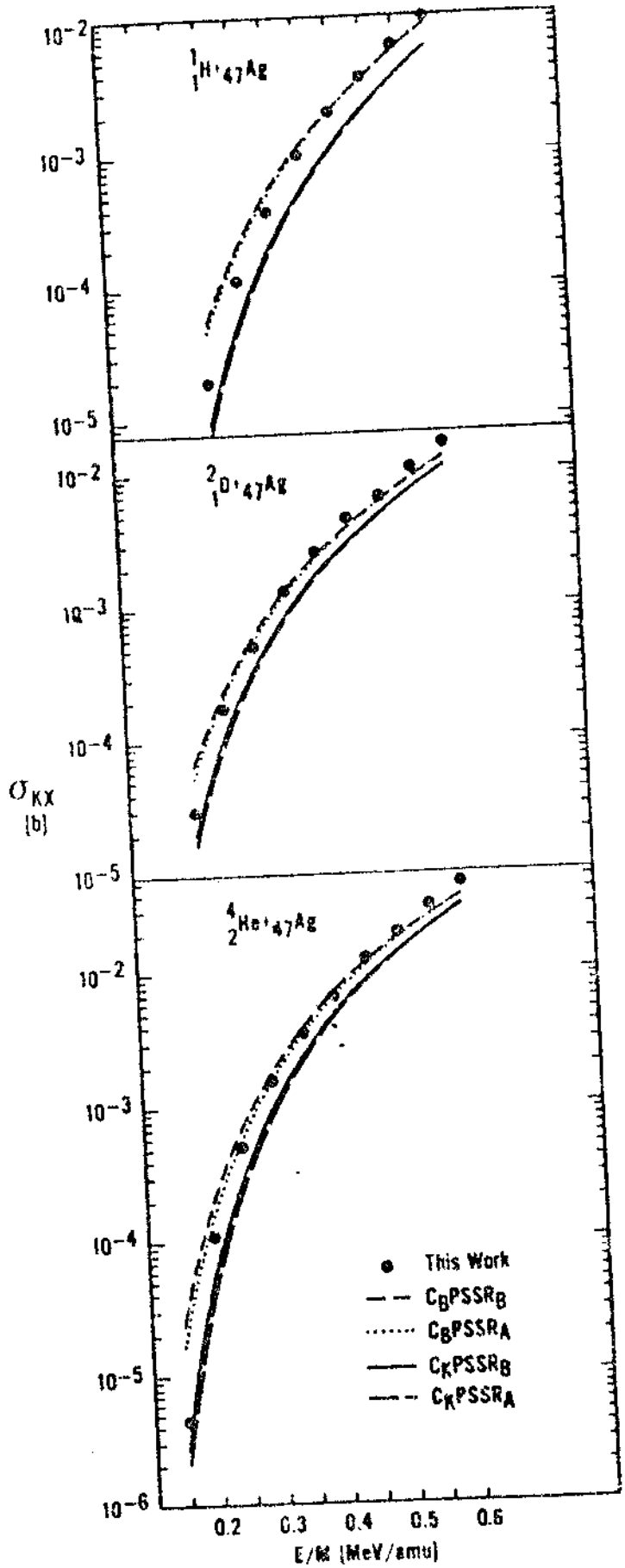

Fig. 5--Measured K-Shell X-Ray Production Cross Sections Compared to Theoretical Predictions of the C_KPSSR_A, C_KPSSR_B, C_BPSSR_A, and C_BPSSR_B for $^{1}_{1}H$, $^{2}_{1}D$, and $^{4}_{2}He$ Ions Incident on $_{47}Ag$.

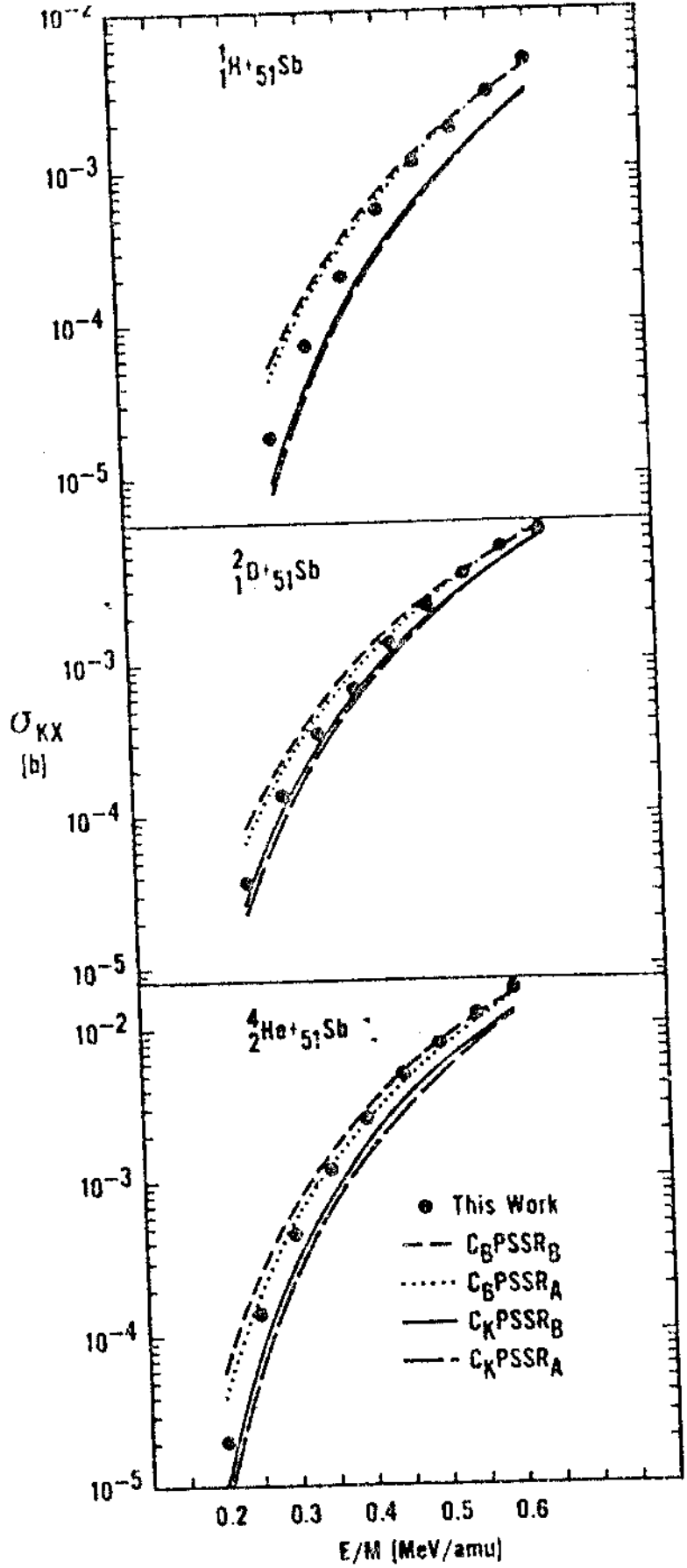

Fig. 6--Measured K-Shell X-Ray Production Cross Section Compared to Theoretical Predictions of the C_KPSSR_A, C_KPSSR_B, C_BPSSR_A, and C_BPSSR_B for $^{1}_{1}H$, $^{2}_{1}D$, and $^{4}_{2}He$ Ions Incident on $_{51}Sb$.

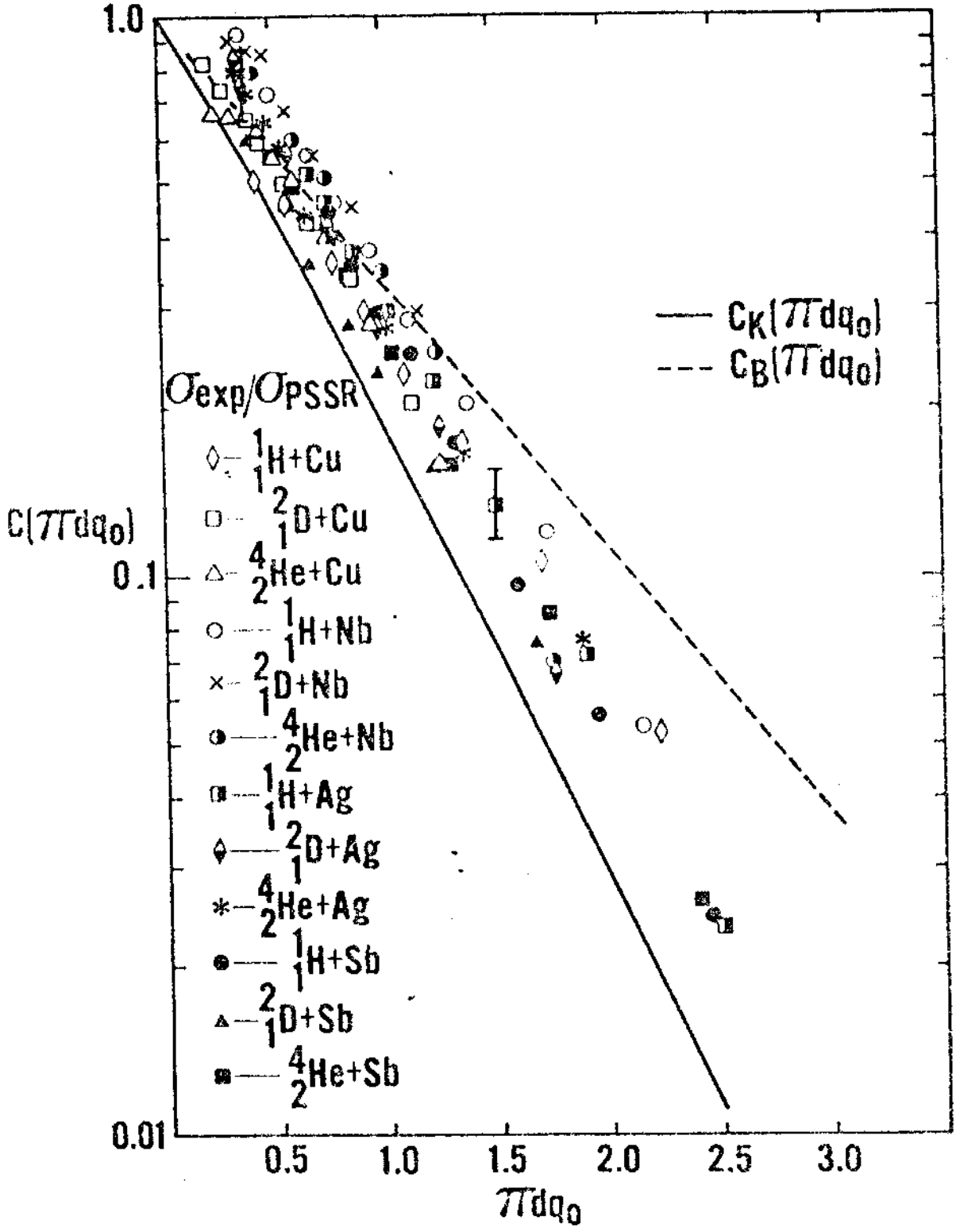

Fig. 7--Experimentally Derived Coulomb Deflection Factor ($\sigma_{exp}/\sigma_{PSSR}$) Compared to Theoretical Predictions of C_K and C_B Versus πdq_o.

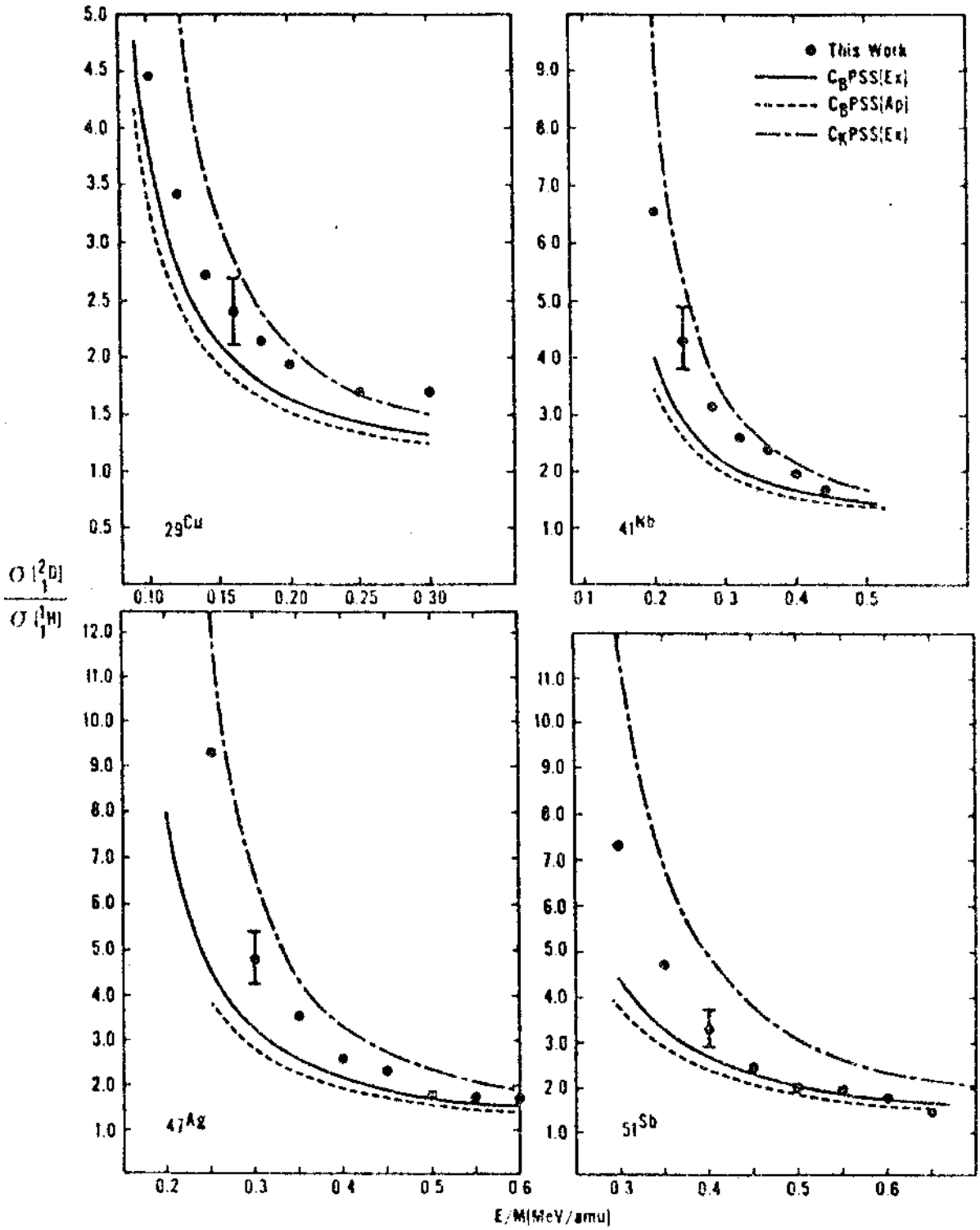

Fig. 8--Measured $\sigma(^2_1D)/\sigma(^1_1H)$ for $_{29}Cu$, $_{41}Nb$, $_{47}Ag$, and $_{51}Sb$ Compared to Theoretical Predictions of the C_BPSS(Ex), C_BPSS(Ap), and C_KPSS(Ex).

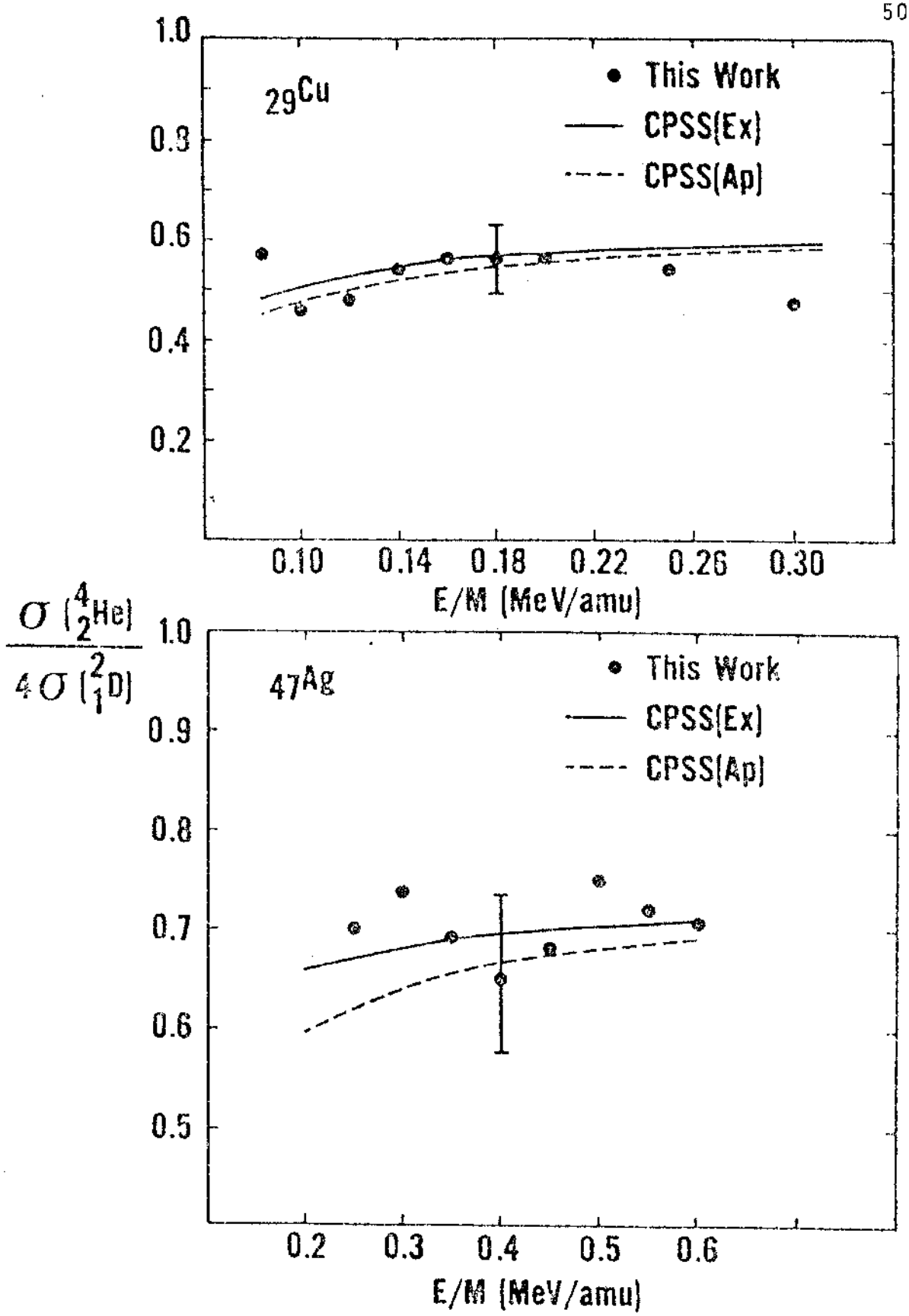

Fig. 9--Measured $\sigma(^4_2\mathrm{He})/4\sigma(^2_1\mathrm{D})$ for $_{29}$Cu and $_{47}$Ag Compared to Theoretical Predictions of CPSS(Ex) and CPSS(Ap).

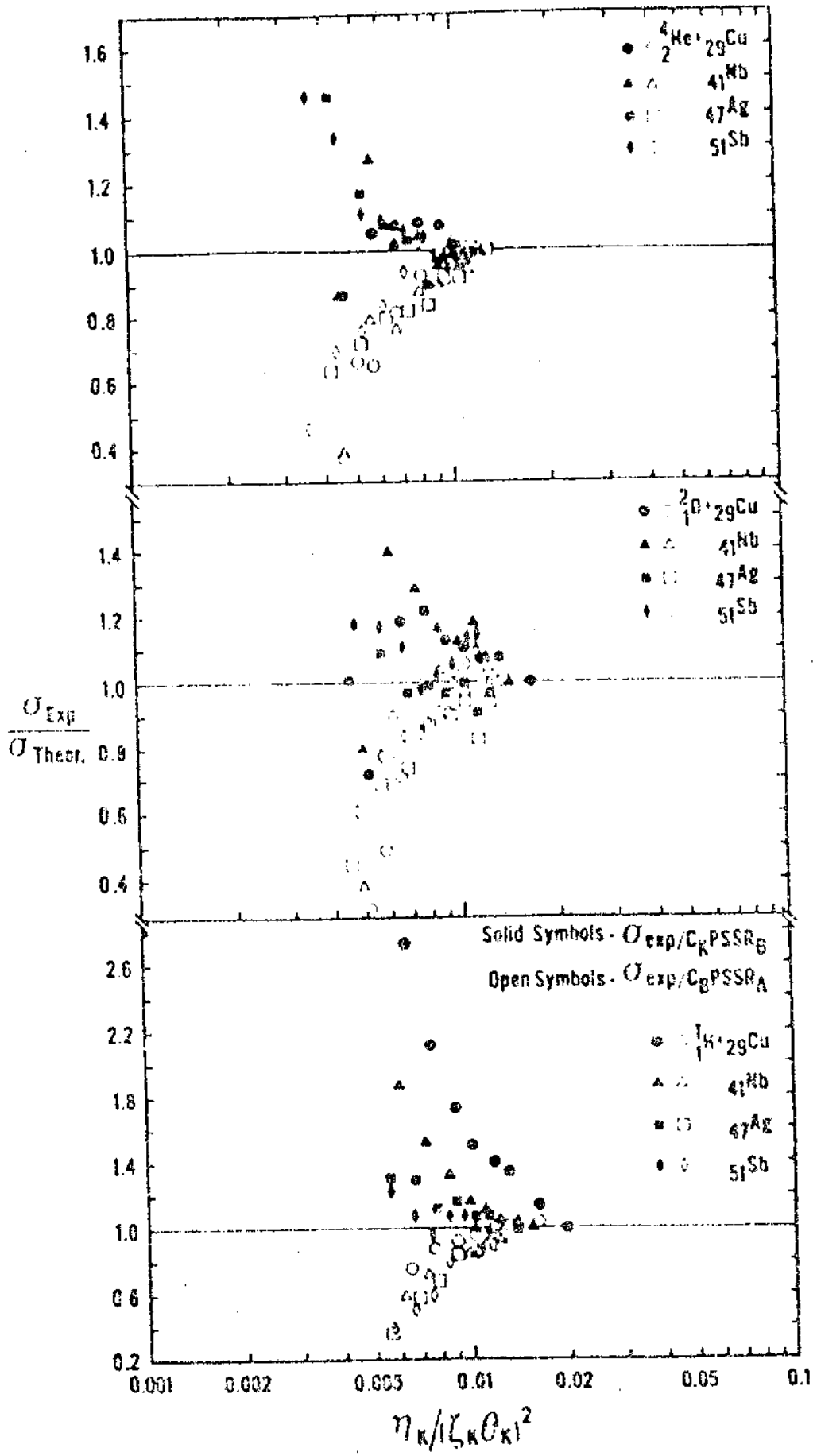

Fig. 10--Ratio of σ_{exp} to σ_{Theor} Normalized to Unity at the Highest Values of $\eta_K/(\zeta_K\theta_K)^2$.

REFERENCES

1. H. A. Bethe, Ann. Physik 5, 325 (1930) and H. A. Bethe, Z. Physik 76, 293 (1932).
2. D. Jamnik and C. Zupancic, Mat. Fys. Medd. Dan. Vid. Selsk. 31, No. 2 (1957).
3. E. Merzbacher and H. Lewis, Encyclopedia of Physics, edited by S. Flugge (Springer-Verlag, Berlin, 1958), Vol. 34, p. 166.
4. J. Bang and J. M. Hansteen, Kgl. Danski Videnskab.
5. U. Fano and W. Lichten, Phys. Rev. Lett. 14, 627 (1965).
6. G. S. Khandelwal, B. H. Choi, and E. Merzbacher, At. Data 1, 103 (1969).
7. B. K. Thomas and J. D. Garcia, Phys. Rev. 179, 94 (1969).
8. J. D. Garcia, E. Gerjuoy, and J. W. Welker, Phys. Rev. 165, 66 (1968); J. D. Garcia, Phys. Rev. A 1, 1402 (1970); 1, 280 (1970).
9. B. H. Choi, Phys. Rev. A 4, 1002 (1971).
10. G. Basbas, W. Brandt, R. Laubert, and A. Schwarzschild, Phys. Rev. Lett. 27, 171 (1971).
11. G. Basbas, W. Brandt, and R. Laubert, Phys. Rev. Lett. 34A, 277(1971).
12. M. Barat and W. Lichten, Phys. Rev. A 6, 211 (1972).
13. G. Basbas, W. Brandt, and R. Laubert, Phys. Rev. A 7, 983 (1973).
14. J. S. Hansen, Phys. Rev. A 8, 822 (1973).

15. See, for example, T. L. Criswell and T. J. Gray, Phys. Rev. A 10, 1145 (1974), N. A. Khelil and T. J. Gray, Phys. Rev. A 11, 893 (1975), and R. Lear and T. J. Gray, Phys. Rev. A 8, 2469 (1973).

16. J. D. Garcia, R. J. Fortner, and J. M. Kavanagh, Rev. Mod. Phys. 45, 111 (1973).

17. J. M. Hansteen and O. P. Mosebekk, Z. Physik 234, 281 (1970); Nucl. Phys. A 201, 541 (1973).

18. J. H. McGuire and P. Richard, Phys. Rev. A 8, 1374 (1973).

19. G. Bissinger, P. H. Nettles, S. M. Shafroth, and A. L. Waltner, Phys. Rev. A 10, 1932 (1974).

20. F. D. McDaniel, T. J. Gray, and R. K. Gardner, Phys. Rev. A 11, 1607 (1975).

21. F. D. McDaniel, T. J. Gray, R. K. Gardner, G. M. Light, J. L. Duggan, H. A. Van Rinsvelt, R. D. Lear, G. H. Pepper, J. W. Nelson and A. R. Zander, Phys. Rev. A 12, 1271 (1975).

22. G. Basbas, Proc. of the Fourth Inter. Conf. on Scientific and Industrial Applications of Small Accelerators, Denton, Texas, 1976. Edited by J. L. Duggan, and I. L. Morgan (IEEE, New York, 1976), p. 142.

23. T. J. Gray, P. Richard, R. L. Kauffman, T. C. Holloway, R. K. Gardner, G. M. Light, and J. Guertin, Phys. Rev. A 13, 1344 (1976).

24. G. Lapicki and W. Losonsky, Phys. Rev. A 15, 896 (1977).

25. F. D. McDaniel, J. L. Duggan, P. D. Miller, and G. D. Alton, Phys. Rev. A 15, 846 (1977).

26. F. D. McDaniel, J. L. Duggan, G. Basbas, P. D. Miller, and G. Lapicki, Phys. Rev. A 16, 1375 (1977).

27. R. Rice, G. Basbas, and F. D. McDaniel, At. Data and Nucl. Data Tables, 20, 503 (1977).

28. J. Tricomi, J. L. Duggan, F. D. McDaniel, P. D. Miller, R. P. Chaturvedi, R. M. Wheeler, J. Lin, K. A. Kuenhold, L. A. Rayburn, S. J. Cipolla, Phys. Rev. A 15, 2269 (1977).

29. S. R. Wilson, F. D. McDaniel, J. R. Rowe, and J. L. Duggan, Phys. Rev. A 16, 903 (1977).

30. R. Anholt, Phys. Rev. A 17, 976 (1978).

31. R. Anholt, Phys. Rev. A 17, 983 (1978).

32. G. Basbas, W. Brandt, and R. Laubert, Phys. Rev. A 17, 1655 (1978).

33. C. Bauer, R. Mann, and W. Rudolph, Z. Physik A 287, 27 (1978).

34. O. Benka and M. Geretschlager, Z. Physik A 284, 29 (1978).

35. R. K. Gardner and T. J. Gray, At. Data and Nucl. Data Tables, 21, 515 (1978).

36. J. C. Slater, Phys. Rev. 36, 57 (1930).

37. R. Rice, M. S. Thesis (North Texas State University, Denton, Texas) 1977.

38. J. C. Ashley, R. H. Ritchie, and W. Brandt, Phys. Rev. B5, 2393 (1972).

39. K. W. Hill and E. Merzbacher, Phys. Rev. A9, 156 (1974).

40. J. Bang and J. M. Hansteen, Mat-Fys. Medd. 31, 13 (1959).

41. Handbook of Mathematical Functions, edited by Milton Abramowitz and Irene a. Stegun (NBS, 1964) p. 81.

42. L. Kocbach, Phys. Norv. 8, 187 (1976).

43. W. Brandt and G. Lapicki, Phys. Rev. A 20, 465 (1979).

44. L. B. Magnusson, Phys. Rev. 107, 161 (1957); R. J. Gehrke and R. A. Lokken, Nucl. Instrum. Methods 97, 219 (1971); J. S. Hansen, J. C. McGeorge, D. Nix, W. D. Schmidt-Ott, I. Unus, and R. W. Fink, Nucl. Instrum. Methods 106, 365 (1973); J. L. Campbell and L. A. McNelles, Nucl. Instrum. Methods, 117, 519 (1974); 125, 205 (1975).

45. J. F. Ziegler, Hydrogen: Stopping Powers and Ranges in All Elemental Matter, (Pergamon Press, New York, 1977); J. F. Ziegler, Helium: Stopping Powers and Ranges in All Elemental Matter, (Pergamon Press, New York, 1977).

46. R. Laubert, H. Haselton, J. R. Mowat, R. S. Peterson, and I. A. Sellin, Phys. Rev. A 11, 135 (1975).

47. W. Bambynek, B. Craseman, R. W. Fink, H. U. Freund, H. Mark, C. D. Swift, R. E. Price, and P. V. Rao, Rev. Mod. Phys. 44, 716 (1972).

48. J. S. Lopes, A. P. Jesus, S. C. Ramos, private communication.